The Effect of Higher Order Moments in the Post-Newtonian Gravitational Wave Expansion on Parameter Estimation

by

Terrence J. Torres

Submitted to the Department of Physics
in partial fulfillment of the requirements for the degree of

Bachelor of Science in Physics

at the

MASSACHUSETTS INSTITUTE OF TECHNOLOGY

June 2008

Author .....
Department of Physics
May 16, 2008

Certified by .....
Dr. Scott A. Hughes
Assistant Professor
Thesis Supervisor

Accepted by .....
David E. Pritchard
Senior Thesis Coordinator, Department of Physics

The Effect of Higher Order Moments in the Post-Newtonian Gravitational Wave Expansion on Parameter Estimation

by

Terrence J. Torres

Submitted to the Department of Physics
on May 16, 2008, in partial fulfillment of the
requirements for the degree of
Bachelor of Science in Physics

Abstract

The purpose of this thesis is to investigate both the qualitative and quantitative effects of including higher order amplitude terms in the post-Newtonian expansion for gravitational waves on parameter estimation of inspiraling binary systems. First, we review the mechanism behind gravitational wave production and the formalism behind our estimation of parameters given a specific waveform. Then, we use a Monte Carlo simulation of 1000 separate binary systems with random position, and orientation parameters and fixed mass ratios between binary objects to generate gravitational waveforms measurements from a detector model which mimics data received from the proposed LISA mission. After that we numerically estimate how well those parameters are determined. The data presented compares median values of accuracy defined as $\Delta\xi/\xi$ for parameters ξ of luminosity distance, chirp mass, and reduced mass, as well as the major and minor axes of a localization ellipse between waveform models which include only the leading quadrupole harmonic amplitude contribution, and the .5PN amplitude harmonic correction to the quadrupole. Our results show that, for all the Monte Carlo simulations run, there is a substantial global improvement in accuracy of the estimated parameters when higher order .5PN amplitude terms are included in the waveform model. The largest improvement shown comes from the range of masses between 10^5 and 10^6 solar masses, which is the ideal reception band for the LISA detector array. This improvement can eventually be applicable to aid in the location of binary sources for confirmation of direct gravitational wave observation. We conclude from these results that it is indeed advantageous to include higher order terms in the post-Newtonian expansion for gravitational wave models in order to obtain more accurate parameter estimates.

Thesis Supervisor: Dr. Scott A. Hughes
Title: Assistant Professor

Acknowledgments

I would like to thank Scott Hughes for his continually helpful advice and support during the length of this work, as well as a large body of numerical routines which he and Ryan Lang have developed and given me access to so that I may build upon them.

Contents

List of Figures

List of Tables

Chapter 1

Introduction

One of the key features of general relativity is its prediction of gravitational waves. The Einstein field equation, which represents a set of differential equations over the metric, have wave solutions both in the presence and absence of mass. Gravitational waves are created by dynamical, non-symmetric, massive systems in which the curvature of spacetime around the system fluctuates with time. This fluctuation creates a waveform that propagates through spacetime, much as any electromagnetic wave propagates through space. Unlike electromagnetic radiation, gravitational waves do not scatter when propagating through matter. By observing these gravitational waves, we stand to gain a better understanding of the dynamics of systems both far away and dark with respect to the electromagnetic spectrum.

Gravitational waves are described as a time dependent perturbation to a slowly varying background metric, $g^{\mathrm{B}}_{\mu\nu}$. One can study the dynamics of these spacetimes by requiring that our perturbative expansion be a solution to the Einstein field equation. We treat the metric perturbation as small and truncate the expansion to a first order term, $h_{\mu\nu}$. With small $h_{\mu\nu}$, we typically then can expand the field equation solutions perturbatively. Though not necessary, it is common for pedagogical reasons to treat the background as the Minkowski metric, $\eta_{\mu\nu} = \mathrm{diag}(-1, 1, 1, 1)$ which describes the geometry of flat spacetime in special relativity [5].

Though there is a strong body of evidence supporting the existence of gravitational waves, direct observation is quite difficult. As they propagate through space,

gravitational waves act as tidal forces on massive bodies, alternately stretching and squeezing along axes perpendicular to the direction of propagation. Because gravity is the weakest of the four fundamental forces, the magnitude of these tidal forces is typically extremely small. Direct observation of gravitational waves requires us to engineer highly precise experiments such as LIGO and LISA.

In this thesis we will specifically focus our attention on the LISA mission, though the later analysis is easily adaptable to the LIGO experiment. LISA is a spaced-based gravitational detector array which will consist of three massive detector components following geodesics in solar orbit. When the mission is launched, the three detector components will be positioned such that their geodesic paths around the Sun will form an equilateral triangle and maintain relative distances between one another. Since the relative distances are maintained, we can then use them as the base points for a three-armed interferometric detector array, where each arm is positioned at 60° relative to the adjacent arms. We hope that this mission will bring about direct observation of gravitational waves from binary systems.

Binary systems are well understood sources which tend to give some of the highest amplitude gravitational waves. In these systems, two massive bodies orbiting one another are the source of asymmetric fluctuations in spacetime curvature.These fluctuations are gravitational waves; this radiation can perform work on other massive bodies, carrying with it energy from the binary system. The radiative energy loss from the production of gravitational waves decreases the mean orbital distance between the two objects in the binary, lowering the time it takes for the two bodies to revolve around one another, and thereby causing normal circular orbits to become slow inspirals. The orbital frequency slowly "chirps" upward as the bodies come together, until finally terminating when the members of the binary eventually coalesce into a single body.

Binary systems which are strong gravitational wave sources must be compact, and so typically contain neutron stars or black holes. Massive binary black hole systems (in which the member black holes are each roughly $10^6\,M_\odot$) in particular appear to form quite commonly as a consequence of the way in galaxies form and grow [11].

Radiative solutions to the Einstien field equations can be fully described by two polarizations. As with Electromagnetism, each polarization is in turn described by a multipolar expansion. Both the monopole and dipole moments, describing the total mass-energy and momentum of the source respectively, cannot radiate due to conservation of energy and momentum. For gravitational radiation, the leading radiative multipole is the quadrupole moment of the source's mass-energy distribution. Since the quadrupole moment is the leading radiative multipole, it typically dominates a source's radiation spectrum. Other terms in the series are often ignored.

Each polarization of a gravitational waveform depends on parameters of the binary system. These include but are not limited to the distance from the binary to the observer, the mass of each of the objects in the binary, the vectors which describe the binary's orientation and position relative to the observer, and the orbital frequency of the binary at the beginning of observation. Using numerical methods it is possible to invert any specific gravitational wave form as a function of these describing parameters. Thus, given both wave polarizations we determine a set of parameters which could have produced the input waveform. In the presence of noise, this determination is not precise, and so we really determine a manifold of parameters all of which could have have produced that waveform (and noise). Ideally, we would like the uncertainty in parameter measurements to be small enough that we can accurately describe the source which generated the waves that we have measured. This translates to one wanting the volume in parameter space which describes waveforms consistent with a measurement to be as small as possible.

Recently, it has been discovered that parameter errors can be reduced by including corrections to the theoretical description of the waveform that correspond to precession effects induced by the spin of a binary's members [3][10]. This increases the accuracy of prediction that we can make as to the possible values for describing parameters of the system. This of course motivates us to ask whether or not we might observe a similar increase in the precision of our parameter predictions by including higher order correction terms to the multipole expansion of a gravitational wave model.

This thesis is concerned with what increase in precision, if any, we achieve by including higher order harmonics in the multipole expansions of the gravitational wave polarizations. Assuming each individual harmonic describes its own manifold in parameter space upon numerical inversion, we can take the superposition of several terms in the expansion to be the intersection of several manifolds. The possibility exists that such an intersection of the set of those manifolds, derived from the higher order terms in the multipole expansion, may have smaller volume in parameter space than the manifold defined by including only the quadrupole harmonic. This decrease in volume would allow us to more accurately estimating the intrinsic parameters of a radiating source. Ultimately our goal here is to compare parameter estimations over a large number of binary systems for a given input waveform computed by using two separate waveform models. One which includes and the other which excludes higher order multipole harmonics.

Chapter 2

Theory

2.1 Gravitational Radiation

We begin this thesis by reviewing the basic properties of gravitational waves in general relativity as discussed in Ref. [5]. First, we shall show how they arise as wave solutions to the Einstein field equation. Next we shall show that their tidal influence, as described by the Riemann curvature tensor, is gauge invariant. Finally, we will choose a convenient gauge for our calculations and solve the Einstein field equation in that gauge to show that there are indeed wave solutions.

2.1.1 The Linearized Einstein Equations

In linearized theory, gravitational waves can be described as a plane wave evolutions of the metric perturbation given in the weak-field approximation. Let us start by first performing a perturbative approximation to the metric by introducing a metric perturbation. Here we shall do this expansion around a flat spacetime background described by the Minkowski metric, but in fact this process is more general and we could just as easily have expanded around a general background metric. The decomposition is as follows:

$$g_{\mu\nu} = \eta_{\mu\nu} + h_{\mu\nu} \tag{2.1}$$

where $\eta_{\mu\nu}$ =diag(-1,1,1,1) is the standard Minkowski metric and $h_{\mu\nu}$ is the metric perturbation and we take $|h_{\mu\nu}| \ll 1$.

The equations governing the perturbation $h_{\mu\nu}$ are found by computing the Einstein field equations in the perturbative limit. The full field equations are given by

$$G_{\mu\nu} = 8\pi T_{\mu\nu} \ , \tag{2.2}$$

where $G_{\mu\nu}$ is the "Einstein curvature tensor" (or just Einstein tensor), constructed from the metric, and $T_{\mu\nu}$ is the stress-energy tensor. The stress-energy tensor describes how matter and matter flows are distributed in spacetime.

We now show how to calculate the Einstein tensor with our metric. The first step is to compute the "connection coefficients," which are the Christoffel symbols

$$\Gamma^{\rho}_{\mu\nu} = \frac{1}{2} g^{\rho\lambda} \Big(\partial_\mu g_{\nu\lambda} + \partial_\nu g_{\lambda\mu} - \partial_\lambda g_{\mu\nu} \Big) \tag{2.3}$$

Substituting our metric and discarding nonlinear terms in $h_{\mu\nu}$, we find

$$\Gamma^{\rho}_{\mu\nu} = \frac{1}{2} \eta^{\rho\lambda} \Big(\partial_\mu h_{\nu\lambda} + \partial_\nu h_{\lambda\mu} - \partial_\lambda h_{\mu\nu} \Big) \tag{2.4}$$

From the connection, we construct the Riemann curvature tensor, which describes the tidal influence of a gravity in general relativity. Given our metric, this tensor is given to linear order by

$$\begin{aligned} R_{\rho\mu\sigma\nu} &= \eta_{\rho\lambda} \partial_\sigma \Gamma^{\lambda}_{\mu\nu} - \eta_{\rho\lambda} \partial_\rho \Gamma^{\lambda}_{\mu\sigma} \\ &= \frac{1}{2} \Big(\partial_\sigma \partial_\mu h_{\rho\nu} + \partial_\nu \partial_\rho h_{\mu\sigma} - \partial_\sigma \partial_\rho h_{\mu\nu} - \partial_\nu \partial_\mu h_{\rho\sigma} \Big) \end{aligned} \tag{2.5}$$

Contracting over the ρ and σ indices yields the Ricci curvature tensor; a further final contraction yields the Ricci scalar:

$$R_{\mu\nu} = \frac{1}{2} \Big(\partial_\sigma \partial_\nu h^{\sigma}_{\mu} + \partial_\sigma \partial_\mu h^{\sigma}_{\nu} - \partial_\mu \partial_\nu h - \Box h_{\mu\nu} \Big) \tag{2.6}$$

$$R = \partial_\mu \partial_\nu h^{\mu\nu} - \Box h \tag{2.7}$$

where $h = h^{\mu}_{\mu}$.

With these components, we can now write down the Einstein field equation

$$G_{\mu\nu} = R_{\mu\nu} - \frac{1}{2}\eta_{\mu\nu}R = 8\pi T_{\mu\nu} \tag{2.8}$$

where we have neglected the cosmological constant term, and by plugging in Eqs. (2.6) and (2.7) into the field equation, we can write down the linearized field equation:

$$\begin{aligned} G_{\mu\nu} &= 8\pi T_{\mu\nu} \\ &= \frac{1}{2}\Big(\partial_\sigma\partial_\nu h^\sigma_\mu + \partial_\sigma\partial_\mu h^\sigma_\nu - \partial_\mu\partial_\nu h - \Box h_{\mu\nu} - \eta_{\mu\nu}\partial_\rho\partial_\lambda h^{\rho\lambda} - \eta_{\mu\nu}\Box h\Big). \end{aligned} \tag{2.9}$$

2.1.2 Gauge Invariance of the Riemann Tensor

In order to make Eq. (2.9) simpler, we note that a gauge transformation is necessary. However, it's not immediately evident that our linearized Riemann tensor is gauge invariant. Thus we must prove that the difference in $g_{\mu\nu}$ brought about by the gauge transformation leaves the Riemann tensor unchanged. When this is the case, the Einstein equations will have solutions which are independent of choice of gauge. Let us first define a gauge transformation under linear theory. The transformation follows the standard procedure for a gauge transformation, with one caveat. We must remember to symmetrize over the two indices. Thus

$$h'_{\mu\nu} = h_{\mu\nu} + \epsilon\frac{1}{2}\big(\partial_\mu\lambda_\nu + \partial_\nu\lambda_\mu\big) \tag{2.10}$$

then

$$\begin{aligned} g'_{\mu\nu} &= g_{\mu\nu} + \epsilon\delta g_{\mu\nu} \\ \delta g_{\mu\nu} &= \big(\partial_\mu\lambda_\nu + \partial_\nu\lambda_\mu\big) \end{aligned} \tag{2.11}$$

and thus the difference in the Riemann tensor is

$$\begin{aligned}\delta R_{\rho\mu\sigma\nu} &= \frac{1}{2}\big(\partial_\sigma\partial_\mu\partial_\rho\lambda_\nu + \partial_\sigma\partial_\mu\partial_\nu\lambda_\rho + \partial_\nu\partial_\rho\partial_\sigma\lambda_\mu + \partial_\nu\partial_\rho\partial_\mu\lambda_\sigma \\ &\quad -\partial_\sigma\partial_\rho\partial_\mu\lambda_\nu - \partial_\nu\partial_\mu\partial_\sigma\lambda_\rho - \partial_\nu\partial_\sigma\partial_\rho\lambda_\mu - \partial_\mu\partial_\rho\partial_\nu\lambda_\sigma\big) \\ &= 0 \end{aligned} \tag{2.12}$$

Thus the Riemann curvature tensor is gauge invariant, and so in order to simplify our calculation we shall make a gauge transformation which will put restrictions on $h_{\mu\nu}$.[5]

2.1.3 The Transverse Traceless Gauge

In order to make our calculation similar we shall make a gauge transformation in the transverse traceless gauge, which is defined by the gauge conditions

$$h^{TT}_{0\nu} = 0 \tag{2.13}$$

$$\eta^{\mu\nu}h^{TT}_{\mu\nu} = 0 \tag{2.14}$$

$$\partial_\mu h^{\mu\nu}_{TT} = 0 \tag{2.15}$$

Using these conditions, as well as assuming no gravitational sources (i.e. $T^{\mu\nu} = 0$), Eq. (2.9) simplifies to

$$\Box h^{TT}_{\mu\nu} = 0 \tag{2.16}$$

which one immediately recognizes as a freely-propagating wave equation. All that's left to do now is to solve this wave equations for metric solutions.

2.1.4 Solving the Wave Equation Without Sources

From Eq. (2.16) we know that the solutions to the metric should satisfy a four dimensional wave equation. Thus, in analogy to problems of a similar type we find plane

wave solutions of the perturbation such that

$$h_{\mu\nu} = A_{\mu\nu} e^{ik_\rho x^\rho} \tag{2.17}$$

Now, we must check that the above set of trial functions for $h_{\mu\nu}$ are indeed solutions to Eq. (2.16). To do this, we simply plug Eq. (2.17) into Eq. (2.16) to obtain

$$\begin{aligned} \Box h^{TT}_{\mu\nu} &= -k^\sigma k_\sigma h^{TT}_{\mu\nu} \\ &= 0 \end{aligned} \tag{2.18}$$

Thus we have nontrivial plane wave solutions for the linearized Einstein equations given that $k^\sigma k_\sigma = 0$; or in other words, the wave vector is null.[1]

The transverse gauge conditions give

$$\begin{aligned} \partial_\mu h^{\mu\nu}_{TT} &= ik_\mu A^{\mu\nu} e^{ik_\sigma x^\sigma} \\ &= 0 \end{aligned} \tag{2.19}$$

so

$$k_\mu A^{\mu\nu} = 0. \tag{2.20}$$

Next, note that Eq. (2.13) implies

$$A_{0\nu} = 0 \tag{2.21}$$

Now, we can find explicit solutions for $h^{TT}_{\mu\nu}$ by rotating our coordinate system such that the wave propagates along the direction of a spatial coordinate axis. So for propagation in the $\hat{k}$ direction, the only nonzero components of the wave vector are

$$\begin{aligned} k^0 &= \omega \\ k^3 &= \omega \end{aligned}$$

[1]This result is good theoretical evidence for the fact that gravitational waves propagate at the speed of light.

and thus Eq. (2.20) gives

$$A_{3\nu} = 0 \tag{2.22}$$

We have thus determined $A_{\mu\nu}$ up to four degrees of freedom. However, the traceless and symmetry conditions for $h^{TT}_{\mu\nu}$ provide an additional two constraints, such that in the end there are only two degrees of freedom.

Restricting ourselves to the transverse traceless gauge allows us to determine that there exist radiative plane wave solutions to the Einstein equations which are dependent upon only two parameters which we shall call $h_+(t)$ and $h_\times(t)$. So by solving for the evolution of the h_+ and $h_\times$ parameters we can fully determine the gravitational wave solutions under linearized theory. This process works in all gauges, we merely choose the transverse traceless gauge for convenience in order to simplify our calculation. However, one may always find transverse traceless pieces of the metric in any gauge and it can be shown that they always describe the radiative degrees of freedom [9].

The same process follows similarly for the solutions of the Einstein equations involving sources. We find that there are two parameters which govern the evolution of all gravitational waves and note, without derivation, that they are the polarization components of the wave.

2.1.5 Solving the Wave Equation with a Source

Let us now focus on the generalized solution to the metric perturbation when the stress-energy tensor, $T^{\mu\nu}$ is non-zero.

When this is the case we can simplify the linearized Einstein tensor in Eq. (2.9) by introducing a trace-reversed metric perturbation

$$\bar{h}_{\mu\nu} = h_{\mu\nu} - \frac{1}{2}h\eta_{\mu\nu}. \tag{2.23}$$

This name is apt because it has the effect of reversing the sign of the trace of the metric perturbation.

From here we are free to choose any gauge we so choose. Thus we shall choose the Lorenz gauge which has as a gauge condition that

$$\partial_\mu \bar{h}^{\mu\nu} = 0 \tag{2.24}$$

Applying this condition we can the see that in the trace reversed case that the Einstein tensor becomes

$$G_{\mu\nu} = -\frac{1}{2}\Box \bar{h}_{\mu\nu} \tag{2.25}$$

and thus, via the Einstein equation we must solve the wave equation

$$\Box \bar{h}_{\mu\nu} = -16\pi T_{\mu\nu} \tag{2.26}$$

which is solved by inverting the d'Alambertian operator to obtain an integral over a Green's function, $G(x^\lambda - y^\lambda)$. So in the end we have that

$$\bar{h}_{\mu\nu}(x^\lambda) = -16\pi \int G(x^\lambda - y^\lambda) T_{\mu\nu}\, d^4y \tag{2.27}$$

Via the choice of gauge we can determine, as we did for the sourceless case that only the position components of the metric perturbation are nonzero. Moreover, the Green's function can be expanded as a series of spherical harmonics to give explicit solutions for the integral. The integral which comprises the first order in the Green's function expansion is the quadrupole moment of the expansion. We will not go into the expansion of the Green's function here, but the process is straightforward and can be found in Ref. [8]. Instead we will present some of the specific consequences of adding higher order harmonic terms later in this thesis.

To first order we can then determine the solution for the metric perturbation as

$$\bar{h}_{ij} = \frac{2}{|\vec{x} - \vec{y}|}\, \ddot{I}_{ij} \tag{2.28}$$

where the denominator represents the standard norm for the 3 vectors $\vec{x}$ (the location of the source) and $\vec{y}$ (the location of the field observation), and $\ddot{I}_{ij}$ is the second time

derivative of the quadrupole moment

$$I_{ij} = \int \rho(\vec{x})\big(x_i x_j - \frac{v^2}{3}\delta_{ij}\big)d^3x. \tag{2.29}$$

with mass density $\rho(\vec{x})$.

2.1.6 Binary Systems

Compact inspiralling binary sources are among the most likely candidates for observation of gravitational radiation from space or Earth based detectors such as the LIGO and LISA experiments. As such, the remainder of this thesis shall be focused on the theory behind the emission and detection of gravitational radiation from these sources.

Similar to the above case of freely propagating gravitational radiation through sourceless spacetime, we will be able to describe the dynamics of the waveform generated by binary systems via two independent polarizations components, h_+ and $h_\times$. However, it is impossible to measure such parameters independently from one another. Thus, from a practical standpoint we must build our theory around our means of detection.

The measured gravitational waveform is generally a linear combination of the waves two polarizations. Let us call this measured waveform $h_{\text{tot}}(t)$. It is the sum of the polarizations independently weighted by antenna response functions F_+ (which describes the antenna's response to a pure + polarization) $F_\times$ (which describes the response to a pure $\times$ polarization). These response functions depend on the relative position and orientation of the gravitational wave source to the detector arms. The measured waveform is then

$$h_{\text{tot}}(t) = F_+(\theta_n, \phi_n, \psi_n)h_+(t) + F_\times(\theta_n, \phi_n, \psi_n)h_\times(t) \tag{2.30}$$

where in this case θ_n and ϕ_n are angle parameters specifying in spherical coordinates the relative position of the binary, in a coordinate frame in which the origin is held at

the detector and the axes are specified relative to vector normal to the detector plane which we label $\hat{n}$. Additionally, ψ_n helps to fix the orientation the angular momentum vector of the binary $\hat{L}$.

In order to simulate such binary systems we need only determine how they evolve under the Einstein equation in linearized theory. Accordingly we can use the solution for the metric perturbation given in Eq. (2.28) in order to determine the two parameters h_+ and $h_\times$. To first order we find that

$$h_+ = 2\left(\frac{\tau}{5}\right)^{5/3}\frac{(\pi f)^{2/3}c\eta}{D_L}\Big[-\big(1+\cos^2(\imath)\big)\Big]\cos(2\phi(t)) \tag{2.31}$$

$$h_\times = 2\left(\frac{\tau}{5}\right)^{5/3}\frac{(\pi f)^{2/3}c\eta}{D_L}\Big[-2\cos(\imath)\Big]\cos(2\phi(t)) \tag{2.32}$$

where D_L is the luminosity distance to the binary source, c is the speed of light, $\tau \equiv 5G(m_1+m_2)/c^3$ is the total mass of the system in units of time, and $\eta \equiv (m_1m_2)/(m_1+m_2)^2$ is the ratio of the reduced mass of the system to the total mass. Moreover, m_1 and m_2 specify the mass of each object in the binary, $\cos(\imath) \equiv \hat{L}\cdot\hat{n}$, $\phi(t)$ is the orbital phase of the binary, and f is the frequency of the gravitational wave. We now have a a way to model the observed waveform from binary sources based on physical parameters of the system. However, our end goal is to determine what effect higher moments beyond the quadrupole moment in the expansions for h_+ and $h_\times$ have on both the evolution of the wave and our ability to accurately predict the ranges for physical parameters which determine the evolution of the wave. As such it is necessary to discuss where these higher order moments come from, and how we shall use them in order to increase our predictive accuracy in numerical simulation.

2.2 Higher Order Moments

Recall that in our analysis for the solution of the metric perturbation in the presence of a massive source, we had to invert the d'Alambertian operator, $\Box$, which gave us a Green's function integral. In the previous analysis, in order to obtain explicit solutions we expanded the Green's function in terms of spherical harmonics, throwing

higher order terms away. However, if we choose not to ignore the higher order spherical harmonics this gives us a series expansion of the metric perturbation. One can therefore determine each integral in the series and thus create a series expansion in h_+ and $h_\times$ in order to reflect higher order contributions to the wave evolution. This process is arduous, but has been done previously by Luc Blanchef in Ref. [6] and thus we will simply state his results here. In general we can decompose $h_{+,\times}(t)$ into terms of separate order in (v/c), such as

$$h_{+,\times}(t) = h^{(0)}_{+,\times}(t) + h^{(1/2)}_{+,\times}(t) + h^{(1)}_{+,\times}(t) + h^{(3/2)}_{+,\times}(t) + \cdots \tag{2.33}$$

We find that all terms involving the "plus" polarization component are dependent upon the cosine of a a phase argument, and all terms involving the "cross" polarization component are dependent upon the sine of a phase argument. As such we may represent both the plus and cross polarizations of a wave by using the following series:

$$h_{+,\times}(t) = \sum_j h^j_{+,\times}(t) = \sum_q \sum_b \left[C^j_b(t)\cos(b\ \phi(t)) + S^j_b \sin(b\ \phi(t))\right] \tag{2.34}$$

where here we shall represent different polarization components of different orders by listing all nonzero components in the sum for that contribute to those components for each specific order. This process will thus be a list for each term of the the expansion in both h_+ and $h_\times$ of time/frequency dependent coefficients C^j_b and S^j_b corresponding to the cosine and sine terms respectively for different orders j, up to (3/2) order in (v/c).

Let the amplitude for each wave component be represented as A^j. Then:

$$
\begin{aligned}
A^{(0)} &= 2\left(\frac{\tau}{5}\right)^{5/3}\frac{(\pi f)^{2/3}c\eta}{D_L}, \\
A^{(1/2)} &= \frac{2\tau^2\pi f c\eta}{25D_L}, \\
A^{(1)} &= 2\left(\frac{\tau}{5}\right)^{7/3}\frac{(\pi f)^{4/3}c\eta}{D_L}, \\
A^{(3/2)} &= 2\left(\frac{\tau}{5}\right)^{8/3}\frac{(\pi f)^{5/3}c\eta}{D_L}.
\end{aligned}
$$

The nonzero C_b^a and S_b^a corresponding to each order for the separate polarization components depend on the A^j as follows:

$\boxed{h_+^{(0)}(t)}$

$$C_2^{(0)} = A^{(0)}[-(1+\cos^2(\imath))],$$

$\boxed{h_\times^{(0)}(t)}$

$$S_2^{(0)} = A^{(0)}[-2\cos(\imath)],$$

$\boxed{h_+^{(1/2)}(t)}$

$$
\begin{aligned}
C_1^{(1/2)} &= A^{(1/2)}\left[\frac{-\delta\sin(\imath)(5+\cos^2(\imath))}{8}\right], \\
C_3^{(1/2)} &= A^{(1/2)}\left[\frac{-9\delta\sin(\imath)(1+\cos^2(\imath))}{8}\right],
\end{aligned}
$$

$\boxed{h_\times^{(1/2)}(t)}$

$$
\begin{aligned}
S_1^{(1/2)} &= A^{(1/2)}\left[\frac{-3\delta\cos(\imath)\sin(\imath)}{4}\right], \\
S_3^{(1/2)} &= A^{(1/2)}\left[\frac{-9\delta\cos(\imath)\sin(\imath)}{4}\right],
\end{aligned}
$$

$\boxed{h_+^{(1)}(t)}$

$$
\begin{aligned}
C_2^{(1)} &= A^{(1)}\left[\left(\frac{1}{6}\right)\left(19+9\cos^2(\imath)-2\cos^4(\imath)-\eta(19-11\cos^2(\imath)-6\cos^4(\imath))\right)\right], \\
C_4^{(1)} &= A^{(1)}\left[\frac{4\sin^2(\imath)(1+\cos^2(\imath))(1-3\eta)}{3}\right],
\end{aligned}
$$

$\boxed{h_\times^{(1)}(t)}$

$$
\begin{aligned}
S_2^{(1)} &= A^{(1)}\left[\left(\frac{\cos(\imath)}{3}\right)\left(17-4\cos^2(\imath)-\eta(13-12\cos^3(\imath))\right)\right], \\
S_4^{(1)} &= A^{(1)}\left(\frac{8}{3}\right)(1-3\eta)\cos(\imath)\sin^2(\imath),
\end{aligned}
$$

$\boxed{h_+^{(3/2)}(t)}$

$$
\begin{aligned}
C_1^{(3/2)} &= A^{(3/2)}\Big[\Big(\frac{\delta\sin(\imath)}{192}\Big)\Big(57+60\cos^2(\imath)-\cos^4(\imath) \\
&\qquad -2\eta(49-12\cos^2(\imath)-\cos^4(\imath))\Big)\Big], \\
C_2^{(3/2)} &= A^{(3/2)}\Big[2\pi(1+\cos^2(\imath))\Big], \\
C_3^{(3/2)} &= A^{(3/2)}\Big[\Big(\frac{27\delta\sin(\imath)}{384}\Big)\Big(73+40\cos^2(\imath)-9\cos^4(\imath) \\
&\qquad -2\eta(25-8\cos^2(\imath)-9\cos^4(\imath))\Big)\Big], \\
C_5^{(3/2)} &= A^{(3/2)}\Big[\Big(\frac{625\delta\sin(\imath)}{384}\Big)\Big(\sin^2(\imath)(1+\cos^2(\imath))(1-2\eta)\Big)\Big],
\end{aligned}
$$

$\boxed{h_\times^{(3/2)}(t)}$

$$
\begin{aligned}
S_1^{(3/2)} &= A^{(3/2)}\Big[\Big(\frac{\delta\sin(\imath)\cos(\imath)}{96}\Big)\Big(63-5\cos^2(\imath)-2\eta(23-5\cos^2(\imath))\Big)\Big], \\
S_2^{(3/2)} &= A^{(3/2)}\Big[-4\pi\cos(\imath)\Big], \\
S_3^{(3/2)} &= A^{(3/2)}\Big[\Big(\frac{27\delta\sin(\imath)\cos(\imath)}{128}\Big)\Big(67-15\cos^2(\imath)-2\eta(19-15\cos^2(\imath))\Big)\Big], \\
S_5^{(3/2)} &= A^{(3/2)}\Big[\Big(\frac{625\delta\sin(\imath)\cos(\imath)}{128}\Big)\Big(\sin^2(\imath)(1-2\eta)\Big)\Big].
\end{aligned}
$$

We have introduced $\delta \equiv (m_1 - m_2)/M$. Given such moments we can now set up our formalism for parameter estimation.

Chapter 3

Parameter Estimation

A well-established formalism describes how one may go about estimating the parameters which describe a measured signal. We shall now give a brief summary of the components needed for such estimation in the context of our measured signals following Refs. [2], [4], and [7]. We begin by introducing the vector $\vec{\xi}$ whose components ξ^a denote the various parameters that describe our signal — masses, spins, distance to the system, angles on the sky, etc. Our goal is to assess how well these components can be determined by a given measurement. For our analysis, we will focus on massive binary black hole signals as measured by the space-based LISA detector. Our result will be a statement of the error $\Delta\xi^a$ (or in some cases, fractional error $\Delta\xi^a/\xi^a$) that a measurement obtains. To begin, given two signal waveforms $h_1(t)$ and $h_2(t)$, we can define an inner product:

$$(h_1|h_2) \equiv 2\int_0^\infty \frac{\tilde{h}_1^*\tilde{h}_2 + \tilde{h}_1\tilde{h}_2^*}{S_n(f)}\, df \tag{3.1}$$

where $\tilde{h}_1$ and $\tilde{h}_2$ are the Fourier transforms of the signals,

$$\tilde{h}(f) = \int_{-\infty}^{\infty} dt\, e^{2\pi i f t} h(t) \tag{3.2}$$

with $\tilde{h}_1^*$ and $\tilde{h}_2^*$ complex conjugates. The function $S_n(f)$ is the spectral density of noise in the detector. It describes the expected distribution of noise as a function of

frequency that the LISA detector is being designed to achieve. More concretely, if one makes a measurement over a frequency band from f_1 to f_2, then

$$\sigma_n^2 = \int_{f_1}^{f_2} S_n(f) df \tag{3.3}$$

is the mean squared noise obtained in the measurement. Then, for the set of parameters ξ, the probability that a signal we measure in detectors I and II ($m_{\rm I}$ and $m_{\rm II}$) contains a signal with parameters ξ is can be given by

$$p(\xi|m_{\rm I}, m_{\rm II}) = p^{(0)}(\xi) \exp\Big(-\frac{1}{2}\Big((H_{\rm I} - m_{\rm I}|H_{\rm I} - m_{\rm I}) + (H_{\rm II} - m_{\rm II}|H_{\rm II} - m_{\rm II}) \Big)\Big). \tag{3.4}$$

Here, $p^{(0)}(\xi)$ is the probability distribution of ξ and $H_{\rm I,II}$ are the gravitational wave measurements in detectors I and II neglecting noise. We can then find the most likely parameters which describe the source of the measured gravitational radiation by finding the parameter set $\hat{\xi}$ which maximizes Eq. (3.4). Next, we can estimate the error of estimation by expanding Eq. (3.4) around the estimated parameters $\hat{\xi}$. Letting $\lambda_{\rm I,II}(\xi) = (H_{\rm I,II} - m_{\rm I,II}|H_{\rm I,II} - m_{\rm I,II})$, we can expand to get

$$\lambda_{\rm I,II}(\xi) = \lambda_{\rm I,II}(\hat{\xi}) + \frac{1}{2}\partial_a\partial_b\lambda_{\rm I,II}(\hat{\xi})\delta\xi^a\delta\xi^b + \mathcal{O}((\delta\xi^i)^3). \tag{3.5}$$

In the limit of large signal to noise ratio $\partial_a\partial_b\lambda_{\rm I,II}(\hat{\xi}) = (\partial_a H_{\rm I,II}|\partial_b H_{rmI,II})$. This allows us to write the probability distribution in Eq. (3.4) as

$$p(\xi|m_{\rm I}, m_{\rm II}) = p^{(0)}(\xi) \exp\Big(-\frac{1}{2}\Gamma_{ab}\delta\xi^a\delta\xi^b \Big) \tag{3.6}$$

where we have defined $\delta\xi^a \equiv \xi^a - \hat{\xi}^a$ and the Fisher information matrix Γ_{ab} for our set of parameters ξ^a as

$$\Gamma_{ab} \equiv \left(\frac{\partial H_{\rm I}}{\partial\xi^a} \middle| \frac{\partial H_{\rm I}}{\partial\xi^b} \right) + \left(\frac{\partial H_{\rm II}}{\partial\xi^a} \middle| \frac{\partial H_{\rm II}}{\partial\xi^b} \right) \tag{3.7}$$

The inverse of Γ_{ab} defines the covariance matrix Σ^{ab}. From this analysis it follows that

$$\Sigma^{ab} =< \Delta\xi^a \Delta\xi^b > \tag{3.8}$$

where angle brackets denote an average over an ensemble of noise distributions [7]. It follows that diagonal entries mean error in a measured parameter $< (\Delta\xi^a)^2 >= \Sigma^{aa}$, and off-diagonals define the correlation between parameters.

Using this we can determine the fractional error ratio, $\Delta\xi^a/\xi^a$. Consequently, in order to determine the effect higher moments have on parameter estimation we must first Fourier transform the gravitational waveform with higher order harmonics included. We then find the derivatives with respect to the signal parameters of the Fourier transformed wave functions, calculate and invert the Fisher information matrix. Finally, we compare the $\Delta\xi^a/\xi^a$ values for waveforms with the quadrupole moment only, and those with higher harmonics included.

3.1 The Stationary Phase Approximation

All harmonics of the total waveform have the form $D_a(t) = A_a(t)\cos(a\phi(t))$ up to phase. If $\frac{d\ln A_a}{dt} \ll \frac{d\phi(t)}{dt}$ and $\ddot{\phi}(t) \ll (\dot{\phi}(t))^2$ then we can use the stationary phase approximation to approximate the Fourier transform of each harmonics individually as:

$$\tilde{D}_a(f) \approx \sqrt{\frac{\pi}{2a}} A_a(f) \Big(\frac{d^2\phi}{dt^2}\Big)^{-1/2} \exp[i(2\pi f t(f) - a\phi(f) - \pi/4)] \tag{3.9}$$

Given df/dt and A_a we then have all the information we need to construct the fourier transform of all wave harmonics. Defining a phase factor for each harmonic as

$$\Psi_a(f) = 2\pi f t(f) - a\,\phi(f) - \frac{\pi}{4} \tag{3.10}$$

then we can construct the total waveform as a sum of each harmonic terms indexed by a which corresponds to the coefficient multiplying the phase as

$$\tilde{h}(f) = \sqrt{\frac{\pi}{2}}\left(\frac{d^2\phi}{dt^2}\right)^{-1/2} \sum_{a=1}^{\infty} \frac{1}{\sqrt{a}} A_a(f) e^{i\Psi_a(f)} \tag{3.11}$$

though practically we are only concerned with a of order unity.

3.2 Constructing the Waveform Explicitly

It is useful now to reparametrize our waveform in terms of two mass coefficients, the chirp mass, and the reduced mass, where

$$\mathcal{M} = \eta^{3/5} M\,, \qquad \mu = \eta M \tag{3.12}$$

are the chirp mass, and reduced mass respectively; and

$$\begin{aligned} M &= m_1 + m_2, \\ \mu &= \frac{m_1 m_2}{M}, \\ \eta &= \frac{\mu}{M}. \end{aligned} \tag{3.13}$$

$$\tag{3.14}$$

Under this parametrization up to 2PN post-Newtonian order in (v/c) we have

$$\begin{aligned} \frac{df}{dt} &= \frac{96}{5\pi\mathcal{M}^2}(\pi\mathcal{M}f)^{11/3}\left[1 - \left(\frac{743}{336} + \frac{11}{4}\eta\right)(\pi M f)^{2/3} + (4\pi - \beta)(\pi M f)\right. \\ &\quad \left. + \left(\frac{34103}{181144} + \frac{13661}{2016}\eta + \frac{59}{18}\eta^2 + \sigma\right)(\pi M f)^{4/3}\right] \end{aligned} \tag{3.15}$$

where β is a spin-orbit parameter, and σ is a spin-spin parameter. We then integrate

to obtain

$$\phi(f) = \frac{1}{2}\Bigg(\phi_c - \frac{1}{16}(\pi\mathcal{M}f)^{-5/3}\Bigg[1 + \frac{5}{3}\left(\frac{743}{336} + \frac{11}{4}\eta\right)(\pi Mf)^{2/3} - \frac{5}{2}(4\pi - \beta)(\pi Mf) + 5\left(\frac{3058673}{1016064} + \frac{5429}{1008}\eta + \frac{617}{144}\eta^2 + \sigma\right)(\pi Mf)^{4/3}\Bigg]\Bigg) \tag{3.16}$$

$$t(f) = t_c - \frac{5}{256}\mathcal{M}(\pi\mathcal{M}f)^{-8/3}\Bigg[1 + \frac{4}{3}\left(\frac{743}{336} + \frac{11}{4}\eta\right)(\pi Mf)^{2/3} - \frac{8}{5}(4\pi - \beta)(\pi Mf) + 2\left(\frac{3058673}{1016064} + \frac{5429}{1008}\eta + \frac{617}{144}\eta^2 + \sigma\right)(\pi Mf)^{4/3}\Bigg] \tag{3.17}$$

where t_c and ϕ_c are constants of integration corresponding to the coalescence, defined formally as the moment when $f \to \infty$.[4]

Our $\Psi_a(f)$ then becomes

$$\Psi_a(f) = 2\pi f t_c - \frac{\phi_c}{2} - \frac{\pi}{4} + \frac{3}{128}(\pi\mathcal{M}f)^{-5/3}\Bigg[\frac{(4a-5)}{3} + \frac{20(a-1)}{9}\left(\frac{743}{336} - \frac{11}{4}\eta\right)(\pi Mf)^{2/3} - \frac{(10a-8)}{3}(4\pi - \beta)(\pi Mf) + \frac{10(2a-1)}{3}\left(\frac{3058673}{1016064} + \frac{5429}{1008}\eta + \frac{617}{144}\eta^2 + \sigma\right)(\pi Mf)^{4/3}\Bigg] \tag{3.18}$$

We now have all components necessary to assemble our waveform up to arbitrary order, assuming that we compute the angle dependent amplitude contributions. So from here, to obtain the Fisher information matrix entries we must therefore take derivatives with respect to the parameters ξ.

3.3 Derivatives

Here we shall take the derivatives of seven total parameters, generalizing the process in Ref. [4]:

$$\xi^i = (\ln D_L, t_c, \phi_c, \ln\mathcal{M}, \ln\eta, \beta, \sigma) \tag{3.19}$$

This process is straightforward, but somewhat tedious. The results are:

$$\begin{aligned}
\partial_1\tilde{h} &= \tilde{h}, \\
\partial_2\tilde{h} &= 2\pi i f\tilde{h}, \\
\partial_3\tilde{h} &= -\frac{ia}{2}\tilde{h}, \\
\partial_4\tilde{h} &= -\frac{5i}{128}(\pi\mathcal{M}f)^{-5/3}(A_4 + B_4v^2 - C_4v^3 + D_4v^4)\tilde{h}, \\
\partial_5\tilde{h} &= -\frac{i}{96}(\pi\mathcal{M}f)^{-5/3}(A_5v^2 - B_5v^3 + C_5v^4)\tilde{h}, \\
\partial_6\tilde{h} &= \frac{i(10a-8)}{128}\eta^{-3/4}(\pi\mathcal{M}f)^{-2/3}\tilde{h}, \\
\partial_7\tilde{h} &= -\frac{5i(2a-1)}{256}\eta^{-4/5}(\pi\mathcal{M}f)^{-1/3}\tilde{h}.
\end{aligned} \tag{3.20}$$

We have $v \equiv (\pi Mf)^{1/3}$, and

$$\begin{aligned}
A_4 &= \frac{4a-5}{3}, \\
B_4 &= \frac{4(a-1)}{3}\left(\frac{743}{336} + \frac{11}{4}\eta\right), \\
C_4 &= \frac{2(10a-8)}{15}(4\pi - \beta), \\
D_4 &= \frac{(4a-2)}{3}\left(\frac{3058673}{1016064} + \frac{5429}{1008}\eta + \frac{617}{144}\eta^2 + \sigma\right), \\
A_5 &= (a-1)\left(2\frac{743}{336} - \frac{33}{4}\eta\right), \\
B_5 &= \frac{9(10a-8)}{20}(4\pi - \beta), \\
C_5 &= 6(2a-1)\left(\frac{3058673}{1016064} - \frac{5429}{4032}\eta - \frac{617}{96}\eta^2 - \sigma\right).
\end{aligned} \tag{3.21}$$

Chapter 4

Analysis and Results

4.1 Calculation

For practical purposes, though this process is completely general up to arbitrary post-Newtonian order, we shall only include the (1/2) order terms in our calculation as a proof of concept that the higher order harmonics do indeed improve parameter estimation accuracy. We note that a ranges from 1 to 3. For these calculations we use the LISA experiment as a model for our detector setup, taking there to be two detector arms which have received a measurement. For this model, the space-based LISA detector mission will include 3 detector satellites which hold orbits to form an equilateral triangle. Now, taking there to be two detector arms, our full signal in each detector arm is scaled by a factor of $\sqrt{3}/2$ from the 60° angle between detector arms. Our full signal decomposition is then, in the time domain,

$$\begin{aligned} h_{\rm tot}(t) &= \frac{\sqrt{3}}{2}\Big(F_{\rm I}^{+}(\theta_n,\phi_n,\psi_n)h_{\rm I}^{+}(t) + F_{\rm I}^{\times}(\theta_n,\phi_n,\psi_n)h_{\rm I}^{\times}(t) \\ &\quad + F_{\rm II}^{+}(\theta_n,\phi_n,\psi_n)h_{\rm II}^{+}(t) + F_{\rm II}^{\times}(\theta_n,\phi_n,\psi_n)h_{\rm II}^{\times}(t)\Big) \end{aligned} \tag{4.1}$$

where

$$
\begin{aligned}
F_{\mathrm{I}}^{+}(\theta_n,\phi_n,\psi_n) &= \frac{1}{2}\left(1+\cos^2\theta_n\right)\cos 2\phi_n\cos 2\psi_n \\
&\quad -\cos\theta_n \sin 2\phi_n \sin 2\psi_n \qquad (4.2)\\
F_{\mathrm{I}}^{\times}(\theta_n,\phi_n,\psi_n) &= \frac{1}{2}\left(1+\cos^2\theta_n\right)\cos 2\phi_n\sin 2\psi_n \\
&\quad +\cos\theta_n \sin 2\phi_n \cos 2\psi_n \qquad (4.3)\\
F_{\mathrm{II}}^{+}(\theta_n,\phi_n,\psi_n) &= F_{\mathrm{I}}^{+}\left(\theta_n,\phi_n-\frac{\pi}{4},\psi_n\right) \qquad (4.4)\\
F_{\mathrm{II}}^{\times}(\theta_n,\phi_n,\psi_n) &= F_{\mathrm{I}}^{\times}\left(\theta_n,\phi_n-\frac{\pi}{4},\psi_n\right) \qquad (4.5)
\end{aligned}
$$

as given by Ref. [3].

We then calculate the total Fisher information matrix as a sum of terms over a in each detector

$$\Gamma_{ij}^{\mathrm{Tot}} = \sum_{a=1}^{3}\left(\Gamma_{ij}^{\mathrm{Ia}} + \Gamma_{ij}^{\mathrm{IIa}}\right) \qquad (4.6)$$

We can then invert this to obtain the measurement errors

$$\Delta\xi^i = \sqrt{(\Gamma_{\mathrm{Tot}}^{-1})^{ii}} \qquad (4.7)$$

With the exception of the analytical derivatives performed above, all other calculations are done numerically using C++ with many routines taken from Ref. [3]. The code takes the input parameters, m_1, m_2, redshift (for our purposes this is always $z = 1$, a random number seed, the starting frequency of the Gravitational wave at the beginning of observation (f_0), the period of observation, and the number of binaries in the Monte Carlo simulation ($n = 1000$) in all simulations. Using these parameters the random seed generates 1000 waveform measurements from binary sources with random parameters specifying orientation and luminosity distance. The Fisher matrix is then populated via the derivatives we found in the previous section for each binary in the simulation, and then numerically inverted to obtain the covariance matrix, from which we may calculate the error of estimation. Accuracy is then determined by calculating the ratio of the error obtained from the diagonal elements of the

covariance matrix to the value used for the simulation for a given binary. Then the median value of the 1000 point population is found. From here we can edit the code to generate waveforms using specific harmonics which correspond to the coefficient of phase (what we've called a thus far). Using the same seed across different versions of the code corresponding to different harmonics, we can then compare the median values for the accuracy of the parameter estimation between systems with separate harmonics active. This comparison should give an informative picture as to the effects of higher order harmonics in the post-Newtonian wave expansion by allowing direct comparison of results.

4.2 Results

Here we run various Monte Carlo simulations to calculate median accuracy of parameter estimations for model waveforms. All waveform models used have corrective post-Newtonian terms to 2PN order in the phase and time components, where as we choose three separate cases for the amplitude expansions. The first case incorporates the full .5PN corrections including both $a = 1$ and $a = 3$ parts in the summation, in addition to the standard leading order quadrupole (0PN) term with $a = 2$. The second case contains no corrective terms in amplitude corresponding to only the quadrupole (0PN) moment. Finally, the last case incorporates only the $a = 1$ amplitude term from the .5PN correction, in addition to the standard leading order quadrupole term with $a = 2$. This will allow direct comparison of estimation data to determine the accuracy improvement given by different terms in the amplitude expansion. To do this comparison it is most instructive to look at several different mass ratios when running simulations amongst the three cases because the .5PN correction terms with $a = 1, 3$ have amplitudes which depend on the parameter $\delta \equiv (m_1 - m_2)/M$. Thus as the mass ratio increases, so should the relative amplitudes of the .5PN corrective terms, and thus their effect on the accuracy of parameter estimations. The simulations here were run using one of three mass ratios: $q \equiv m_1/m_2 = \frac{0.55}{0.45} = 1.22 \approx 1$, $q = 3$, and $q = 10$. We have chosen $q \approx 1$ because were q equal to one, then δ would be zero and we would

see no effect from the correction via .5PN terms. Amongst these mass ratios we use as input masses in the $q \approx 1$ case on the order of 10^4 and 10^5. For the $q = 3$ case, our trials involved mass orders of 10^5, 10^6, and 10^7. And finally amongst those cases with $q = 10$, we have the highest mass in the system with order 10^5 and 10^6. With these test cases we've chose to examine specifically the median values for $\Delta\mathcal{M}/\mathcal{M}$; $\Delta\mu/\mu$; $\Delta D_L/D_L$; the major axis estimation, $2l_a$; and the minor axis estimation, $2l_b$. The last two parameters designate the elliptical localization of the source from estimation of the orientation parameters. Improvement in such parameters would help greatly in the visual observation of binary sources from detected gravitational waves. The data from all numerical simulations for the median values of all these parameters is summarized in Tables 4.1, 4.2, and 4.3.

Table 4.1: Median errors in several quantities for 1000 binary Monte Carlo simulation with various masses always in the ratio of $q \approx 1$, $q = 3$, and $q = 10$; including only the quadrupole harmonic (or that is to say using only the 0PN waveform model).

$m_1(M_\odot)$	$m_2(M_\odot)$	$\Delta\mathcal{M}/\mathcal{M}$	$\Delta\mu/\mu$	$\Delta D_L/D_L$	$2l_a$ (arcmin)	$2l_b$ (arcmin)
4.5×10^4	5.5×10^4	3.29×10^{-5}	0.0109	0.0254	159.05	104.44
4.5×10^5	5.5×10^5	0.000124	0.0266	0.0125	93.410	58.503
3.0×10^5	1.0×10^5	5.86×10^{-5}	0.0112	0.0171	114.15	71.027
3.0×10^6	1.0×10^6	0.00118	0.135	0.0132	98.940	56.259
3.0×10^7	1.0×10^7	0.0258	0.642	0.213	1400.7	740.8
1.0×10^5	1.0×10^4	3.73×10^{-5}	0.00653	0.0311	214.99	132.70
1.0×10^6	1.0×10^5	0.000153	0.0178	0.0156	105.37	64.132

The smaller the number in the ratio $\Delta\xi/\xi$ terms represents a greater accuracy in parameter estimation. Similarly, as a general guideline we can evaluate the lowering of the predicted values for $2l_a$ and $2l_b$ to be an increase in localization accuracy of the sky position of the binary. An intuitive comparison of the localization accuracy between sets of data can be gained by evaluating what decrease, if any, there is for the total area of the ellipse. Unfortunately this measure of accuracy does not take into account practical search implementation for binaries. Specifically, it is possible for a highly eccentric ellipse to localize the binary into a fairly small area of the sky; however, the presence of high eccentricity makes for a difficult search procedure since

Table 4.2: Median errors in several quantities for 1000 binary Monte Carlo simulation with various masses always in the ratio of $q \approx 1$, $q = 3$, and $q = 10$; and including all higher harmonics up to .5PN order.

$m_1(M_\odot)$	$m_2(M_\odot)$	$\Delta\mathcal{M}/\mathcal{M}$	$\Delta\mu/\mu$	$\Delta D_L/D_L$	$2l_a$ (arcmin)	$2l_b$ (arcmin)
4.5×10^4	5.5×10^4	$1.62 \times 10{-}5$	0.00422	0.0237	154.17	99.577
4.5×10^5	5.5×10^5	4.51×10^{-5}	0.00616	0.00844	76.277	49.087
3.0×10^5	1.0×10^5	2.14×10^{-5}	0.00258	0.00781	69.075	45.250
3.0×10^6	1.0×10^6	0.000261	0.0200	0.00562	55.230	39.898
3.0×10^7	1.0×10^7	0.0117	0.610	0.00688	52.595	43.690
1.0×10^5	1.0×10^4	1.46×10^{-5}	0.00162	0.0259	196.01	125.20
1.0×10^6	1.0×10^5	4.76×10^{-5}	0.00341	0.00903	80.143	51.764

Table 4.3: Median errors in several quantities for 1000 binary Monte Carlo simulation with various masses always in the ratio of $q \approx 1$, $q = 3$, and $q = 10$; including only the the terms in the post-Newtonian expansion of the waveform corresponding to the harmonics with 1 and 2 as coefficients of the phase.

$m_1(M_\odot)$	$m_2(M_\odot)$	$\Delta\mathcal{M}/\mathcal{M}$	$\Delta\mu/\mu$	$\Delta D_L/D_L$	$2l_a$ (arcmin)	$2l_b$ (arcmin)
4.5×10^4	5.5×10^4	3.07×10^{-5}	0.0102	0.0251	157.52	102.26
4.5×10^5	5.5×10^5	5.72×10^{-5}	0.00987	0.00994	83.505	53.459
3.0×10^5	1.0×10^5	2.74×10^{-5}	0.00401	0.0101	90.259	53.769
3.0×10^6	1.0×10^6	0.000332	0.0261	0.00754	68.927	43.628
3.0×10^7	1.0×10^7	0.0121	0.610	0.0128	93.233	61.704
1.0×10^5	1.0×10^4	2.52×10^{-5}	0.00409	0.0291	204.98	129.86
1.0×10^6	1.0×10^5	5.44×10^{-5}	0.00427	0.0113	91.593	58.084

telescopes search in circular sections. Consequently it may be possible for a larger area of the sky to be searched in less time given that the localization is non-eccentric. For a better picture of this, see Figure 4-1. In general this data shows fairly large improvement over nearly all parameters in all cases. To see the percent change given from including all .5PN amplitude terms we refer to Table 4.4. In this table we have defined $\delta_{\Lambda^i} \equiv 100(\Lambda^i_{(0\text{PN})} - \Lambda^i_{(.5\text{PN})})/\Lambda^i_{(0\text{PN})}$, where here

$$\Lambda^i = \left(\frac{\Delta\mathcal{M}}{\mathcal{M}}, \frac{\Delta\mu}{\mu}, \frac{\Delta D_L}{D_L}, 2l_a, 2l_b\right). \tag{4.8}$$

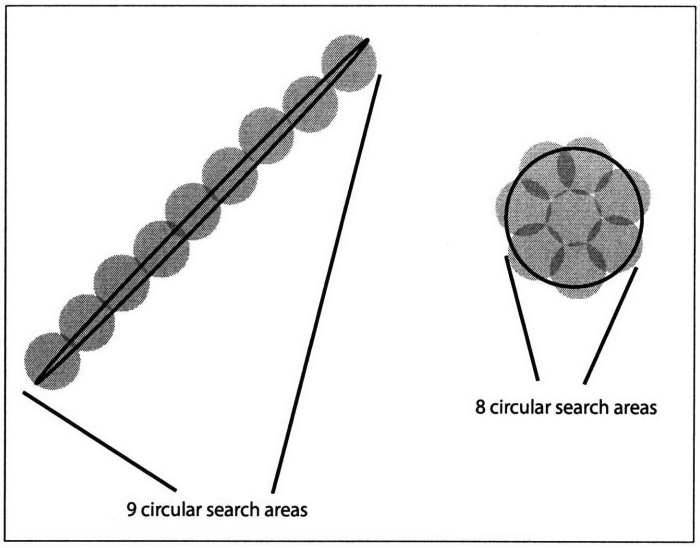

Figure 4-1: The ellipse on the left has lower area and is covered by a greater number of circular areas, thus searching for a binary system within the left ellipse of localization might possibly take a greater amount of time than the right case. This demonstrates that, practically, comparing areas of the localization ellipses is not a good measure of sky position accuracy.

We note that the largest accuracy improvement over all simulations is given over the simulations with binary objects of mass $10^6 M_\odot$. Specifically, for $\Delta\mathcal{M}/\mathcal{M}$, $\Delta\mu/\mu$, and $\Delta D_L/D_L$ the largest improvement falls under the $q = 3$ case with mass terms on the order of $10^6 M_\odot$. And for the major and minor axis improvement, we have the largest improvement in the $q = 3$ case with mass terms on the order of $10^7 M_\odot$. As a general trend it seems that the improvement in accuracy has a peak value for masses on the order of $10^6 M_\odot$ for $\Delta\mathcal{M}/\mathcal{M}$, $\Delta\mu/\mu$, and $\Delta D_L/D_L$. On either side of this mass band for a given mass ratio, q, the accuracy improvement drops off dramatically. This trend is most easily seen in Tables 4.5, 4.6, and 4.7. With all other variables which are non random held fixed, these simulations show a definite spike around $10^6 M_\odot$ over median accuracy improvement from the quadrupole harmonic as the only amplitude term, to the full .5PN amplitude expansion.

There are also interesting trends in the improvement of parameter estimations by separate terms in the .5PN amplitude expansion when we look at the relative improvements of the estimates when only the $a = 1$ and $a = 2$ harmonics are included

Table 4.4: Comparison of the improvement of estimation accuracy, $x^i = \Delta\xi^i/\xi^i$, calculated as a percent change, Λ^i.

$m_1(M_\odot)$	$m_2(M_\odot)$	$\delta_{\mathcal{M}}$	δ_μ	δ_{D_L}	δ_{2l_a}	δ_{2l_b}
4.5×10^4	5.5×10^4	103	158	7.2	3.2	4.9
4.5×10^5	5.5×10^5	175	332	48.1	22.5	19.2
3.0×10^5	1.0×10^5	174	334	119	65.3	57.0
3.0×10^6	1.0×10^6	352	575	135	79.1	41.0
3.0×10^7	1.0×10^7	54.7	5.0	96.8	2563.2	1595.6
1.0×10^5	1.0×10^4	155	303	201	9.7	6.0
1.0×10^6	1.0×10^5	221	422	72.8	31.5	23.9

Table 4.5: Values for parameter estimation accuracy for $\Delta\mathcal{M}/\mathcal{M}$ over $q = 3$ simulations. Quadrupole and PN.5 values compared, along with percent difference δ.

$m_1(M_\odot)$	$m_2(M_\odot)$	$\Delta\mathcal{M}/\mathcal{M}$ (0PN)	$\Delta\mathcal{M}/\mathcal{M}$ (.5PN)	$\delta_{\mathcal{M}}$ (in %)
3.0×10^5	1.0×10^5	0.0000586	0.0000214	174
3.0×10^6	1.0×10^6	0.00118	0.000216	352
3.0×10^7	1.0×10^7	0.0258	0.0117	54.7

in the waveform model relative to the full .5PN expansion model. Particularly, Table 4.8 gives the percent change $\delta^{12}_{D_L}$ for the quadrupole only expansion relative to the expansion with the $a = 1, 2$ harmonics and $\delta^{123}_{D_L}$ gives the relative change between parameter estimates in the quadrupole only expansion and the full .5PN amplitude expansion. By noting that larger differences in $\Upsilon_{D_L} \equiv \delta^{123}_{D_L} - \delta^{12}_{D_L}$ correspond to greater effect in increasing overall accuracy of the $a = 3$ term of the harmonic expansion we can evaluate the importance of its inclusion in the expansion.

We can see from Table 4.8 that improvements gained by adding in the $a = 3$ term are often much larger in the luminosity distance than those gained from just the $a = 1, 2$ harmonic terms. We then expect that the $a = 3$ term play a large role in many of the corrections for the luminosity distance, which can be made sense of intuitively since it is this term which accumulates greater total phase over the course of observation than either of the previous two. In contrast we may look at the decrease in the major and minor axis of localization predictions given by only the

Table 4.6: Values for parameter estimation accuracy for $\Delta\mu/\mu$ over $q = 3$ simulations. Quadrupole and PN.5 values compared, along with percent difference δ.

$m_1(M_\odot)$	$m_2(M_\odot)$	$\Delta\mu/\mu$ (0PN)	$\Delta\mu/\mu$ (.5PN)	δ_μ (in %)
3.0×10^5	1.0×10^5	0.0112	0.00258	334
3.0×10^6	1.0×10^6	0.135	0.0200	575
3.0×10^7	1.0×10^7	0.642	0.610	5.0

Table 4.7: Values for parameter estimation accuracy for $\Delta D_L/D_L$ over $q = 3$ simulations. Quadrupole and PN.5 values compared, along with percent difference δ.

$m_1(M_\odot)$	$m_2(M_\odot)$	$\Delta D_L/D_L$ (0PN)	$\Delta D_L/D_L$ (.5PN)	δ_{D_L} (in %)
3.0×10^5	1.0×10^5	0.0171	0.00781	119
3.0×10^6	1.0×10^6	0.0132	0.00562	135
3.0×10^7	1.0×10^7	0.213	0.00688	96.8

$a = 1, 2$ terms, as opposed to the full .5PN amplitude expansion. In this case, we can see by the data point in which there is greatest improvement (that is for the $q = 3$ sequence with masses on the order of $10^7 M_\odot$) that the $a = 1, 2$ terms contribute the vast majority of improvement and little more is added by including the $a = 3$ term.

Table 4.8: We show the difference in improvement over the full mass trial spectrum for D_L when only the $a = 1, 2$ terms are included in the amplitude expansion and when $a = 1, 2, 3$ are all included.

$m_1(M_\odot)$	$m_2(M_\odot)$	$\delta^{12}_{D_L}$	$\delta^{123}_{D_L}$
4.5×10^4	5.5×10^4	1.2	7.2
4.5×10^5	5.5×10^5	25.8	48.1
3.0×10^5	1.0×10^5	69.3	119
3.0×10^6	1.0×10^6	75.1	135
3.0×10^7	1.0×10^7	15.6	96.8
1.0×10^5	1.0×10^4	6.9	201
1.0×10^6	1.0×10^5	38.1	72.8

Chapter 5

Summary and Conclusion

In summary, in this thesis we have gone though the theory behind gravitational radiation. We have shown that waves can propagate through a sourceless spacetime, as well as being produced from asymmetric fluctuations in the gravitational field. We focus our study on binary sources, and choose a mass regime which is within the LISA detectors prime observation band. The types of binaries which comprise this regime have total masses of roughly on the order of $10^4 - 10^8 M_\odot$ and so we assume that such binaries are comprised of neutron star and black hole interactions (though this fact plays no role in the analysis).

We then review basic signal processing which allows us to estimate parameter sets which are most likely to have produced a gravitational wave measurement. This process requires that we have a model for our gravitational waveform. In past work which concerns parameter estimation, higher order amplitude harmonic terms in the post-Newtonian gravitational wave expansion have been neglected. However, here we focus on the inclusion in our simulations of such higher order terms up to .5PN order and set up a derivative formalism which is easily generalizable to even higher order terms in the expansion for future investigations.

Without the presence of noise in the signal it would be theoretically possible to exactly estimate the system of parameters which maximizes the probability of seeing those parameters in the waveform measurement. However, because of the existence of noise in the signal pathway, we can only determine a parameter up to

some error specification. As such we can estimate the accuracy of our determination by measuring the ratio of that error to the estimated value of that parameter. This gives us a sense of the accuracy to which we can estimate parameters.

By performing a Monte Carlo simulation across 1000 binary systems with random sky position, luminosity distance, and orientation parameters we can find the median accuracy to which our parameters are estimated for projected noise models in the LISA spaced-based detector mission. We then compare the accuracy of determination between waveform models which include amplitude corrections up to the full .5PN order, the amplitude corrections of only the $a = 1$ harmonic term in addition to the quadrupole $a = 2$ term, and the basic quadrupole only model.

We have shown through these simulations that there is an across the board improvement over measurement accuracy for both cases involving corrective amplitude terms in the post-Newtonian expansion. There are also several interesting trends in the data which deserve some discussion. We note primarily the the largest improvement in luminosity distance, chirp mass, and reduced mass occur as a peak in the mass range of $10^6 M_\odot$. Additionally, as mass ratio increases over the same mass order spectrum (here we only compar $10^5 M_\odot$) chirp mass and reduced mass have reduced accuracy, whereas the accuracy in luminosity distance increases with the mass ratio. For the localization ellipse predictions, as a general trend both major and minor axes have increased accuracy over a given mass ratio spectrum for higher mass simulations.

Lastly, we have also investigated the importance of each individual corrective piece of the .5PN order amplitude correction. To do so we compare data from simulations run with only the $a = 1$ corrective term added to the quadrupole moment amplitude and with both $a = 1$ and $a = 3$ terms in the .5PN expansion added tot he quadrupole moment term. We find that chirp mass, distance, and reduced mass are all highly dependent on the effects from the $a = 3$ piece, where as the major and minor axis predictions, in general, show little increased improvement from the contributions of the $a = 3$ harmonic.

This data shows that the inclusion of .5PN corrective terms to the waveform amplitude is largely beneficial to both predictive accuracy of waveform parameters such

as mass and distance, as well as the prediction of orientation and position parameters which allow us to localize the binary position in the sky based on measured gravitational wave observation data. This increase in accuracy could one day aid in the confirmation of measurement data by allowing us to accurately locate and observe a binary system given a gravitational wave measurement.

Finally, since such large improvements can be seen at low and order .5PN corrections, one might gain additional accuracy improvements by including even higher order post-Newtonian corrections. The theory behind the analytical derivatives needed to incorporate such terms is broadly general via scaling; though we leave it for future analysis to include such terms, this analysis should serve as a proof of concept that these corrections are indeed very important in accurately predicting parameters from waveform measurement data.

Bibliography

[1] Curt Cutler and Éanna E. Flanagan, Phys. Rev. D **49**, 2659(1994).

[2] Scott A. Hughes, Mon. Not. R. Astron. Soc. **000**, 1-12 (2001).

[3] Ryan N. Lang and Scott A. Hughes, Phys. Rev. D **74**, 122001 (2006).

[4] Eric Poisson and Clifford M. Will, Phys. Rev. D **52**, 848 (2006).

[5] Sean M. Carroll, *Spacetime and Geometry: An Introduction to General Relativity* (Addison Wesley, San Fransisco, 2004).

[6] Luc BLanchet, Living Rev. Rel. **9** (2006) 4.

[7] L. S. Finn, Phys. Rev. D **46**, 5236 (1992).

[8] Jack Vanderlinde, *Classical Electromagnetic Theory* (Springer, Netherlands, 2004) 155-159.

[9] E. E. Flanagan and S. A. Hughes, New Journal of Physics **7**, 204 (2005).

[10] A. Vecchio, Phys. Rev. D 70, 042001 (2004).

[11] A. Sesana, M. Volonteri, and F. Haardt, M. Not. R. Astron. Soc. **377**, 1711 (2007).